





# From stripes to bubbles: Deterministic transformation of magnetic domain patterns in Co/Pt multilayers induced by laser helicity

Nina Novakovic-Marinkovic <sup>1,2,\*</sup> Mohamad-Assaad Mawass <sup>1,\*</sup> Oleksii Volkov,<sup>3</sup> Pavlo Makushko,<sup>3</sup> W. Dieter Engel,<sup>4</sup> Denys Makarov <sup>3</sup> and Florian Kronast <sup>1</sup>

<sup>1</sup>*Helmholtz-Zentrum Berlin für Materialien und Energie, 12489 Berlin, Germany*

<sup>2</sup>*Institut für Physik und Astronomie, Universität Potsdam, Karl-Liebknecht-Strasse 24/25, 14476 Potsdam, Germany*

<sup>3</sup>*Helmholtz-Zentrum Dresden-Rossendorf e. V., Institute of Ion Beam Physics and Materials Research, 01328 Dresden, Germany*

<sup>4</sup>*Max Born Institute Berlin, Max-Born-Strasse 2A, 12489 Berlin, Germany*



(Received 15 May 2020; revised 14 August 2020; accepted 18 September 2020; published 9 November 2020)

The optical control of magnetism offers an attractive possibility to manipulate small magnetic domains for prospective memory devices on ultrashort time scales. Here, we report on the local deterministic transformation of the magnetic domain pattern from stripes to bubbles in out-of-plane magnetized Co/Pt multilayers controlled only by the helicity of ultrashort laser pulses. Relying on the experimentally determined average size of stripe domains and the magnetic layer thickness, we calculate the temperature and characteristic fields at which the stripe-bubble transformation occurs. Furthermore, we demonstrate that in the narrow range of the laser power, the helicity induces a drag on domain walls.

DOI: [10.1103/PhysRevB.102.174412](https://doi.org/10.1103/PhysRevB.102.174412)

## I. INTRODUCTION

Due to potential applications in magnetic data storage, (ultrafast) optical control of magnetism emerged as a promising technique for the deterministic manipulation of magnetization dynamics and magnetic domain patterns [1–5]. The possibility to reverse the magnetization as a function of the helicity of laser pulses is referred to as all-optical helicity-dependent switching (AO-HDS). Magnetic switching by AO-HDS occurs in many materials from ferrimagnetic rare-earth/transition metal alloys [6,7] to ferromagnetic thin films [6,8–10]. Despite active research in the field of all-optical manipulation of magnetism [6,11–14], questions related to the influence of laser pulses on magnetic domain patterns in out-of-plane magnetized ferromagnetic thin film remain undercovered.

Stripe and bubble domains are observed in many magnetic material systems with perpendicular anisotropy, such as ferromagnets [15–17] and ferrimagnets [18]. In static experiments, the transition between two states can be driven as a function of temperature and/or external magnetic field [15,17,19]. However, up to now there are no reports on the deterministic transition from stripe to bubble domains in dynamic experiments relying on all-optical switching.

Here, we report localized all-optical helicity dependent transformation of stripe into bubble domains, in out-of-plane magnetized Co/Pt multilayer stacks. Within a narrow range of magnetic bias fields, the illumination by ultrafast pulses of circularly polarized laser light results in a purely helicity dependent and reversible transition between stripe and bubble domain patterns. Photoemission electron microscopy

(PEEM) is used for direct imaging of the magnetic domains, exploiting the x-ray magnetic circular dichroism (XMCD) as the magnetic contrast mechanism. We identify two crucial parameters to achieve the deterministic transition between stripe and bubble domains, namely the laser fluence and the strength of an out-of-plane oriented magnetic bias field. We apply the phenomenological bubble theory to describe the evolution of the domain state in magnetic materials with perpendicular magnetic anisotropy exposed to an out-of-plane magnetic field. By knowing micromagnetic parameters of the sample and relying on the experimentally determined average width of a stripe near the stripe saturation field, we estimate the magnetic field equivalent to the laser helicity, as well as the temperature range at which the stripe-bubble transition occurs.

The structure of this paper is as follows. In Sec. II we describe the fabrication and initial characterization of the samples using x-ray-absorption spectroscopy (XAS) and Kerr microscopy. Furthermore, we present the methodology together with the experimental setup used to study the laser-induced magnetization control of domain patterns. In Sec. III, we assess the transformation of magnetic domains as a function of laser helicity and discuss in detail the mechanism behind the stripe-bubble transition. Finally, Sec. IV provides a general conclusion drawn from our experiments. Appendix gives a detailed explanation of derivations used to calculate the characteristic fields and sizes of domains.

## II. EXPERIMENTAL DETAILS

Magnetic layer stacks consisting of Pt(5 nm)/[Co (0.4 nm)/Pt (0.7 nm)] × 5/Pt (2 nm) have been grown on MgO substrates using magnetron sputtering at room temperature (base pressure of  $5 \times 10^{-8}$  mbar); Ar

\*These authors contributed equally to this work.

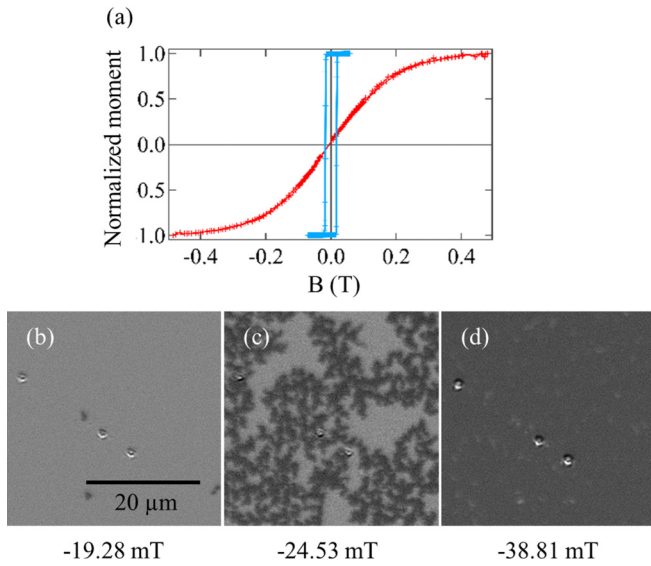


FIG. 1. (a) Magnetic hysteresis loop measured in out-of-plane and in-plane magnetic fields. The square shape of the loop measured in the out-of-plane field with high remanent magnetization suggests that the sample has out-of-plane easy axis of magnetization. (b)–(d) Series of Kerr microscopy images revealing the evolution of the magnetic domain pattern when the sample is exposed to out-of-plane magnetic field of different strength. Black and white color represent two antiparallel out-of-plane magnetic orientations.

is used as a sputter gas at a pressure of  $2 \times 10^{-3}$  mbar; deposition rate 0.5 Å/s. Integral magnetic properties are characterized using a Tensormeter setup [20–22] by means of anomalous Hall effect measurements. The characteristic shape of the hysteresis loops measured in out-of-plane and in-plane magnetic fields [Fig. 1(a)] confirms the out-of-plane easy axis of magnetization.

The evolution of magnetic domain patterns as a function of the applied magnetic field along the easy axis direction is analyzed using a magneto-optical Kerr microscope (Evico Magnetics) [Figs. 1(b)–1(d)]. It is found that small bubbles appear when the magnetically saturated sample is exposed to a reverse magnetic field [Fig. 1(b)]. These bubbles act as nucleation spots branching into labyrinth domains. With the increasing magnetic field, domains change their shape and grow in size [Fig. 1(c)], eventually leaving only islands of remaining domains [white circular domains in Fig. 1(d)]. The position of nucleation points is arbitrary and changes in each magnetization cycle.

AO-HDS experiments are performed at the photoemission electron microscope (SPEEM at UE49PGMa beamline) at BESSY II synchrotron facility at the Helmholtz-Zentrum Berlin [23]. Figure 2(a) shows a sketch of the experimental setup. A Femtolasers Scientific XL Ti:Sa-laser (central wavelength 800 nm; pulse duration 80 fs) is used as an optical pulsing source. A pulse picker placed after the laser output allows setting the repetition rate from 2.5 MHz down to a single pulse. In these experiments, we apply pulse trains of circularly polarized laser pulses at the repetition rate of 1.25 MHz. Assuming Gaussian laser spot, all fluences given in this paper refer to the peak fluence at the center of the laser spot. The circular polarization is established by a quarter-wave

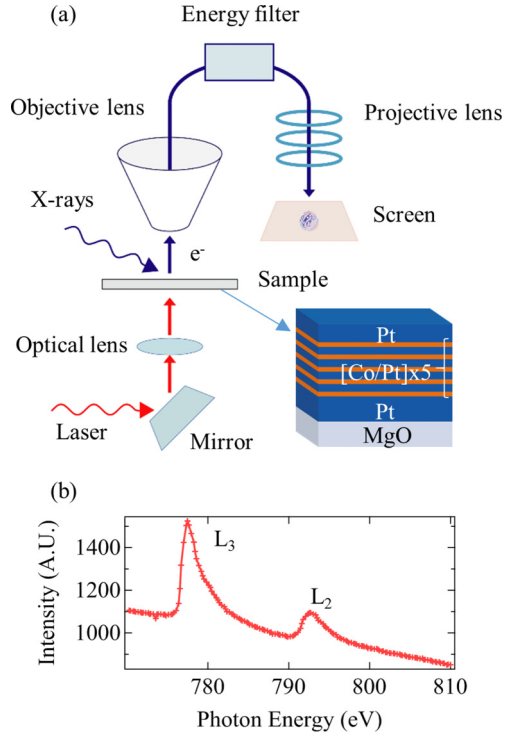


FIG. 2. (a) Apparatus scheme and sample layout. (b) X-ray-absorption spectrum of Co contains a single sharp peak at 777.5 eV confirming that the magnetic layer stack is not oxidized.

plate directly in front of the vacuum port of the PEEM UHV chamber.

The sample is mounted on a sample holder with integrated laser optics and temperature control [24]. This sample holder features a small mirror and lens focusing the laser light normal to the backside of the sample at a spot size of about  $3 \mu\text{m}$ . The out-of-plane magnetic bias field is generated by a solenoid, 6 mm in diameter, centered around the investigated area and mounted in a notch at the surface of the sample holder.

The sample surface is illuminated by the x-ray beam incident at a grazing angle of  $16^\circ$ . The photoemission electron microscope images the lateral photoelectron distribution at the sample surface with a spatial resolution of 30 nm [23].

The magnetic contrast in XMCD-PEEM, is calculated from a series of PEEM images recorded for left and right circularly polarized x-rays ( $c^-$  and  $c^+$ ) at Co  $L_3$  (777.5 eV) absorption edge:  $\text{XMCD} = \frac{I(c^+) - I(c^-)}{I(c^+) + I(c^-)}$  [25]. The Co  $L_2$  and  $L_3$  x-ray-absorption spectrum shows no indication of oxidation [Fig. 2(b)].

### III. RESULTS AND DISCUSSION

#### A. All-optical helicity-dependent switching

Initially the sample is uniformly magnetized in an out-of-plane magnetic field. After applying a laser pulse train of  $6.6 \text{ mJ}/\text{cm}^2$ , the uniform magnetization within the field of view transforms into stripe domains.

To investigate the presence and onset of AO-HDS, we analyze XMCD images recorded during the excitation with opposite laser helicities (Fig. 3). The laser fluence is increased stepwise from 2.3 to  $5.3 \text{ mJ}/\text{cm}^2$ . At a fluence of  $3.4 \text{ mJ}/\text{cm}^2$ ,

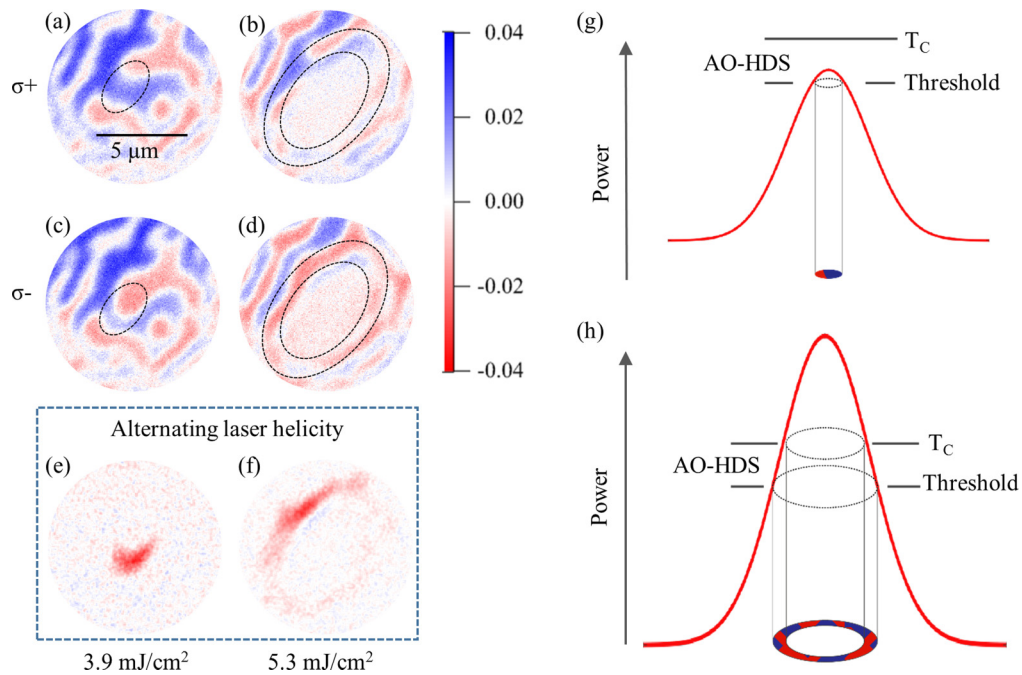


FIG. 3. (a)–(d) XMCD images showing helicity dependent domain-wall motion at different laser fluence. The intensity of the XMCD signal is proportional to the projection of the magnetization  $M$  along the x-ray beam direction  $k$ . Color scale represents two antiparallel out-of-plane orientations of magnetization (red and blue). Domain wall, a nonmagnetic state or an orthogonal magnetic orientation to the x-rays is color coded with white. The laser pulse repetition rate is 1.25 MHz; (e), (f) Average difference between PEEM images (acquired with fixed x-ray polarization) recorded with laser light of opposite helicities. (g), (h) Schematic showing the laser profile and the AO-HDS process.

the change of the laser helicity results in a drag on the domain walls indicating the onset of the AO-HDS process at this fluence. This effect is shown in Figs. 3(a) (for  $\sigma+$ ) and 3(c) (for  $\sigma-$ ) at a laser fluence of 3.9  $\text{mJ}/\text{cm}^2$ , where one magnetic domain orientation grows at expense of the other one, with the opposite orientation, in the center of the laser spot. A local demagnetization process occurs at the fluence of 4.9  $\text{mJ}/\text{cm}^2$ . The demagnetized area is observed in the center of the laser spot and grows with the increase of the laser fluence (images in Figs. 3(b) and 3(d) are taken for laser fluence of 5.3  $\text{mJ}/\text{cm}^2$ ).

The magnetic images in Figs. 3(e) and 3(f) are recorded by alternating the laser helicity at a fixed x-ray helicity. Therefore, the displayed magnetic contrast arises only from the magnetization switching as a function of the laser helicity. Both images clearly show regions in which the local magnetization switches as a function of the laser helicity. The extension of the region reveals that the AO-HDS depends on the laser fluence within the Gaussian laser spot. In Figs. 3(g) and 3(h), a schematic of the laser profile is presented. At low laser fluence, the AO-HDS region appears in the center of the laser spot [Fig. 3(g)]. At higher laser fluences, the sample becomes demagnetized in the inner part of the laser spot due to the excessive laser power. Therefore, the AO-HDS region becomes ring-shaped, indicating a threshold behavior (Fig. 3(h)). Schematic in Fig 3(g)–(h) is presented relative to the critical (thermal demagnetization) temperature. This threshold behavior is explained in detail by Arora *et al.* [14] and has been also observed in a study by Alebrand *et al.* [26]. It has been shown that AO-HDS switching appears between two threshold fluences: The lower threshold fluence describes the

transition from no switching to all-optical switching, while the upper threshold fluence separates the all-optical switching range from the thermal demagnetization range. The minimum fluence for AO-HDS to occur decreases with increasing the laser repetition rate due to accumulated heat.

The origin of helicity dependent switching is still under debate. In combination with the heat arising from the laser pulses, there are two most probable phenomena considered to cause deterministic AO-HDS: inverse Faraday effect (IFE) [11,27] and magnetic circular dichroism (MCD) [28]. Clarifying on which of the two effects is dominant in our system is out of the scope of this study.

## B. Stripe-bubble transition

In the second set of experiments, we investigate the stripe-bubble transition as a function of the laser helicity and magnetic field. Since the AO-HDS is achieved only in a narrow window of the laser fluence [26], instead of moving the laser spot, we sweep the laser fluence from 7.5 to 1.5  $\text{mJ}/\text{cm}^2$ . In this way, the AO-HDS region is moved from outside to the inside of the laser spot, affecting a larger sample area by the threshold laser power. Each time the laser power is swept down, the previous state of the system (bubbles or stripes) is erased by the initially high laser fluence and new state forms as a function of the laser helicity. The resulting domain patterns for such sweeps are shown in Figs. 4(a)–4(c).

The measurements are done for different magnetic bias fields with a strength of 0.24, 0.36, and 0.48 mT, applied along the out-of-plane axis. In the presence of the bias fields of 0.24 mT [Fig. 4(a)] and 0.48 mT [Fig. 4(c)] the resulting domain

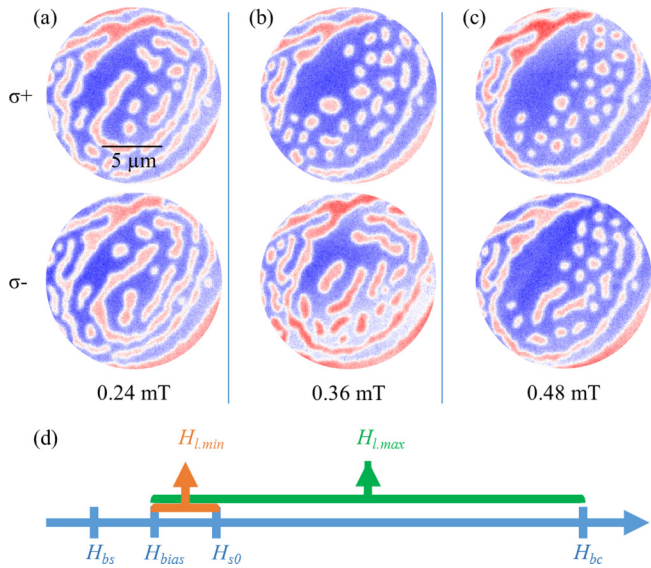


FIG. 4. (a)–(c) XMCD images showing helicity dependent creation and annihilation of bubble domains in nonzero magnetic bias fields applied along the easy axis of the sample. (d) Scheme of the characteristic magnetic fields: strip-out field ( $H_{bs}$ ), stripe saturation field ( $H_{s0}$ ), bubble collapse field ( $H_{bc}$ ), and lower and upper limits of the magnetic field equivalent to the effective field given by the laser helicity ( $H_{l,min}$  and  $H_{l,max}$ , respectively).

pattern is quite similar for both laser helicities. Depending on the bias field, both helicities cause the formation of mainly stripe or mainly bubble domains, respectively. However, at an intermediate bias field of 0.36 mT [Fig. 4(b)], the domain pattern is very different for opposite laser helicities. While bubble domains are formed for  $\sigma+$  laser helicity,  $\sigma-$  helicity results in mostly stripe domain pattern. Similar behavior is observed at negative bias fields, though at a bias field of  $-0.36$  mT the helicity effect is inverted, with  $\sigma+$  causing stripe and  $\sigma-$  the bubble domains to form.

The existence of the upper and lower bias fields, at which the laser helicity induced switching between stripe and bubble domains is overruled by the magnetic bias field, and the fact that the helicity effect inverts in an opposite bias field suggest that the influence of the laser helicity acts equivalent to an external magnetic field. The magnetic pattern obtained at 0.36 mT bias field and  $\sigma-$  laser helicity consists mostly of stripe domains, resembling patterns acquired at 0.24 mT bias field. Contrary, when the sample is illuminated with  $\sigma+$  laser helicity at the same bias field, bubble domains are formed, similarly as observed at 0.48 mT bias field. This suggests that for our samples exposed to the laser pulse train at a 1.25 MHz repetition rate, the effect of the laser helicity is equivalent to around 0.12 mT.

In the literature, different values of the equivalent magnetic field induced by a circularly polarized laser pulse can be found ranging from 10 mT to several tens of teslas [29–32]. However, these studies are typically done using single pulse laser excitations of different fs to ps duration. In our experiment, the sample is exposed to a laser pulse train of several seconds, increasing the overall temperature of the system and finally, reducing the saturation magnetization. This may

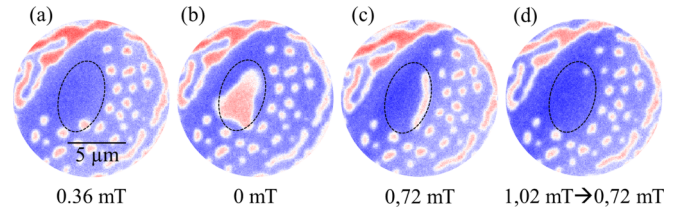


FIG. 5. XMCD images showing the change in the domain pattern at different strength of the magnetic bias field, constant laser helicity and fluence of  $3.59$  mJ/cm<sup>2</sup>. In the last image, the magnetic field is swept down from 1.02 to 0.72 mT and then the sample was imaged. The position of the laser spot is indicated in the image.

lead to much smaller estimated effective field compared to previous research. A small bias field is necessary to stabilize magnetic bubble domains. However, the field range accessible to our setup (maximum of 1.33 mT) is not sufficient for the field driven stripe-bubble transition to occur. In contrast to the data shown in Fig. 4, Fig. 5 shows a series of XMCD images that are recorded at different bias fields, and at fixed laser helicity and fixed laser fluence of  $3.6$  mJ/cm<sup>2</sup>, which is below the demagnetization threshold. Starting from the bubble state at 0.36 mT bias field [Fig. 5(a)], the bias field is reduced to 0, causing the bubble closest to the laser spot to expand [Fig. 5(b)]. On the other hand, if the bias field is increased to 0.72 mT, the bubble transforms into a stripe domain, which further transforms to a much smaller bubble domain at higher fields [Figs. 5(c) and 5(d)]. Please note that other bubble domains at further distance from the laser spot remain unchanged.

Je *et al.* [33] suggest that it is necessary to overcome a magnetostatic energy barrier for bubbles to occur. This barrier is large compared to  $k_bT$ . Therefore, a transition between stripe and bubble magnetic domain patterns cannot happen just by applying small magnetic fields. A temperature increase close to  $T_C$  produced by the laser is required to provide sufficient energy to the system. The decrease of the saturation magnetization leads to lowering the energy barrier and, depending on the strength of the magnetic field and laser helicity, enables bubble or stripe domains to form [33,34]. This scenario is applicable to the case shown in Fig. 4, where the initial laser power is sufficiently high to demagnetize the area within the laser spot. During the decrease of the laser power, the magnetic domain pattern is first formed in the presence of the applied bias field and the laser helicity. As the temperature is further lowered and the energy barrier increased, the magnetic pattern freezes.

From our findings, we conclude that the transition from stripe to bubble domains via circularly polarized laser light is a cooperative effect between the magnetic bias field, laser helicity and temperature. This conclusion is in good agreement with the study done by Medapalli *et al.* [9].

### C. Bubble theory estimations

Finally, we employ a phenomenological bubble theory [35,36] to understand better the influence of the effects of magnetization relaxation and temperature on our results. The theory allows calculating magnetic fields characterizing the

stability of isolated bubbles. These characteristic fields are (i) the strip-out field  $H_{bs}$ , at which bubble spontaneously expands into stripe domain, (ii) the saturation field for stripes  $H_{s0}$ , above which only bubble domains exist, and (iii) the collapse field  $H_{bc}$ , above which bubble domains are no longer stable.

The characteristic fields are strongly temperature dependent as the saturation magnetization  $M_s$  strongly changes with temperature. Experimentally extracted sample parameters are the magnetic layer thickness ( $t = 5.5$  nm), saturation magnetization at room temperature ( $M_s = 0.75 \times 10^6$  A/m) and the average width of a stripe near the stripe saturation field ( $H_{s0}$ ), which amounts to ( $W = 0.76$   $\mu$ m). To obtain this average width, several stripes from the transitional regime between stripes and bubbles in Fig. 4 are measured.

Since the domains form at temperatures close to the Curie temperature  $T_C$ , their relative domain width  $\omega_r = W/t$  can be used to derive the characteristic length of the material ( $l_c = 9.5$  nm) at that temperature (see the Appendix). For the stripe-bubble transition to occur at 0.36 mT the temperature has to be around 97% of the  $T_C$ . At this temperature the calculated fields for  $H_{bs}$  and  $H_{s0}$  amount to 0.34 and 0.38 mT, respectively. This means that below 0.34 mT only stripe domains exist and above 0.38 mT stripes are saturated while bubble domains are still present. As the temperature decreases, the saturation magnetization increases, leading to the increase of the strength of the characteristic fields. Below this temperature no changes of the magnetic pattern are observed. We note that while the theory assumes that the system is at constant temperature in the experiment, the laser pulse train results in temperature oscillations. Therefore, the local temperature at least temporarily has to reach around 97% of  $T_C$  to enable the helicity driven stripe-bubble transition. This estimate is in good agreement with the observation that the stripe-bubble transition can only occur close to the demagnetization threshold. The transient temperature could also be calculated directly for a specific laser power, for example using the two-temperature model [37]. However, due to the Gaussian laser spot, the exact position where the stripe-bubble transition occurs is difficult to determine, which is likely to result in a large error in the temperature estimation.

The characteristic magnetic field calculated based on the bubble theory can be used further to estimate the magnetic field  $H_l$ , equivalent to the laser helicity. At the bias field,  $H_{bias}$ , of 0.36 mT, laser pulses with positive helicity resulted in the stabilization of bubble domains only. This means that  $H_{bias} + H_l \geq H_{s0}$ . At the same time, laser pulses with negative helicity resulted in stripe domains only. This means that  $H_{bias} - H_l \leq H_{bs}$  [Fig. 4(d)]. Hence, the lower limit of the magnetic field equivalent of the laser helicity is 0.02 mT. The upper limit can be calculated from the bubble collapse field ( $H_{bc}$ ). At this field bubbles are no longer stable, which means that the effective field arising from the laser helicity cannot be higher than that field. From the calculations, this field amounts to 0.56 mT, leading to the upper limit of 0.2 mT. However, these limits do not fully agree with the experimental results. This can be due to high pinning of domain wall on the sample inhomogeneities. Alternatively, it can also be due to the presence of the surrounding bubbles [36]. Nevertheless, estimated field range agrees with the experimentally determined value 0.12 mT.

#### IV. CONCLUSION

We demonstrate experimentally a laser helicity dependent switching between magnetic stripe and bubble domain states in Co/Pt multilayers with out-of-plane easy axis of magnetization. We directly image the evolution of the magnetic domain patterns using the XMCD-PEEM technique upon illumination of the sample with a train of laser pulses at 1.25 MHz repetition rate. The observed deterministic transition between two magnetic states is a result of the cooperative effect between the magnetic bias field, laser helicity, and thermal heating of the sample to temperatures close to  $T_C$ . By comparing the influence of the laser helicity on magnetic domains at different bias fields, we find that the effect of the laser helicity is equivalent to a dc magnetic field of 0.12 mT. We apply a phenomenological bubble theory to calculate the lower and upper boundaries of the magnetic field equivalent to the laser helicity, which amount to 0.02 and 0.2 mT, respectively. For these estimations it is necessary to assume that the temperature in the area where the size of the bubble changes reaches about 97% of the  $T_C$ .

The possibility of addressing the magnetic state of individual bubbles is fundamental in magnetic data storage technologies, specifically, localized control of bubble domain formation, annihilation, and manipulation. Our results show that it is possible to use the effect of helicity dependent switching to realize the deterministic transitioning between different magnetic domain patterns, as well as to manipulate individual domains. These findings enable further investigations of conditions in which the formation and annihilation of individual bubble domains in an ultrafast manner could be achieved using optical techniques.

#### APPENDIX

The approximations for phenomenological bubble theory calculations are taken from [35] and [36]:

(i) The sample possesses an out-of-plane easy axis of magnetization. The shape anisotropy ( $K_d$ ), uniaxial magnetic anisotropy ( $K_u$ ), and exchange parameter ( $A$ ) are determined at room temperature and amount to 0.35 MJ/m<sup>3</sup>, 0.51 MJ/m<sup>3</sup>, and 4.5 pJ/m, respectively. From here, the quality factor  $Q$  is calculated to be 1.45, which indicates that the magnetic easy axis points perpendicular to the surface plane.

(ii) The sample has a uniform thickness  $t$  and its lateral dimensions are infinite.

(iii) The magnetic field  $H$  is applied parallel to the surface normal.

(iv) The thickness of the plate is assumed to be small enough so that the domain structure can be considered to consist of straight domains, and the 180° Bloch walls are perpendicular to the surface. Moreover, domains are always large compared to the Bloch wall width.

Beyond the saturation field, the stripes do not collapse into an equilibrium bubble lattice, but into as many bubbles as there were independent stripe segments. In this case bubbles can be treated as an independent entities and bubble theory for isolated bubble domains can be used [35]. The total energy of

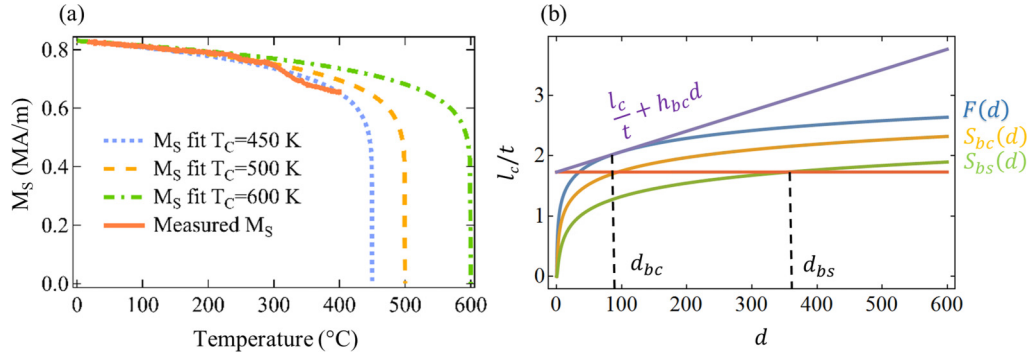


FIG. 6. (a) Measured and fitted saturation magnetization as a function of temperature. (b) A diagram to derive the bubble stability conditions.

an isolated bubble domain is

$$e_{\text{tot},b} = 2\pi K_d t^3 \left( -I(d) + \frac{l_c}{t}d + \frac{1}{2}hd^2 \right), \quad (\text{A1})$$

where  $d = 2R/t$  is the reduced bubble diameter ( $R$  being the bubble radius) and  $I(d) = -\frac{2}{3\pi}d[d^2 + (1-d^2)E(u)/u - K(u)/u]$  is the stray field energy gain by the bubble. We approximate the Co/Pt multilayer stack with a single layer [38], which is 5.5 nm thick.  $E(u)$  and  $K(u)$  are the complete elliptical integrals defined as follows:

$$\begin{aligned} E(u) &= \int_0^{\pi/2} \sqrt{1 - u^2 \sin^2 \alpha} d\alpha, \\ K(u) &= \int_0^{\pi/2} d\alpha / \sqrt{1 - u^2 \sin^2 \alpha}, \end{aligned} \quad (\text{A2})$$

where  $u = \frac{d}{\sqrt{1+d^2}}$ .

The characteristic fields are calculated by formulating the equilibrium conditions: for a reduced applied field  $h = H/M_S$  and a given ratio  $l_c/t$ , the reduced bubble diameter  $d = 2r/t$  must fulfill the condition

$$F(d) = \frac{l_c}{t} + hd, \quad (\text{A3})$$

where  $F(d)$  is the so-called force function. The force function is a derivative of  $I(d)$ :

$$F(d) = \frac{\partial I}{\partial d} = -\frac{2}{\pi}d^2[1 - E(u)/u]. \quad (\text{A4})$$

To calculate the characteristic magnetic field at temperatures near  $T_C$ , the saturation magnetization should be estimated. A superconducting quantum interference device vibrating-sample magnetometer (SQUID VSM) is used to determine the dependence of saturation magnetization on temperature. The temperature dependence was measured by means of a Quantum Design SQUID VSM in an out-of-plane field of 100 mT [Fig. 6(a)]. The saturation magnetization depends on temperature and is fitted by a power law:

$$M_s(T) = M_0 \left( 1 - \frac{T}{T_C} \right)^\beta, \quad (\text{A5})$$

where exponent  $\beta$  is 0.5 from mean field theory [39]. The saturation magnetization at zero temperature,  $M_0$ , is estimated to be 0.83 MA/m. Fitting to the data accordingly to the Curie

law gives an estimate for the Curie temperature to be in the range of 500 K [Fig. 6(a)]. The model is in agreement with the experimental results if the assumed temperature is above 97% of the  $T_C$ , allowing for the saturation magnetization to be calculated.

The characteristic length can be calculated as follows:

$$2\pi \frac{l_c}{t} = \omega_r^2 \ln \left( 1 + \frac{1}{\omega_r^2} \right) + \ln(1 + \omega_r^2),$$

where  $\omega_r = W/t$ . From here,  $l_c$  amounts to 9.5 nm.

A bubble domain of lower or higher density state will develop in an externally applied perpendicular field depending on the nature of the remanent state [35]. As the field is increased, the bubble diameter decreases. The critical field corresponding to the smallest diameter of the bubble domain (collapse diameter) can be determined from the condition that the straight line  $(l_c/t + hd)$  touches the  $F(d)$  curve in one point [Fig. 6(b)]:

$$\begin{aligned} \frac{l_c}{t} = S_{bc}(d) &= F(d) - \frac{d \partial F}{\partial d} \\ &= \frac{2d}{\pi} \left[ d - \sqrt{1 + d^2} E(u) + \frac{u}{d} K(u) \right]. \end{aligned} \quad (\text{A6})$$

The intersection of  $S_{bc}$  with the straight line  $l_c/t$  gives  $d_{bc}$ , from which follows the collapse diameter of the bubble domain  $r_{bc} = 0.52 \mu\text{m}$ . From here, the critical field  $h_{bc}$  is obtained from Eq. (A3) ( $F(d_{bc}) = l_c/t + h_{bc}d_{bc}$ ), and the collapse field amounts to 0.56 mT.

On the other hand, the condition for the stripe-out diameter comes from the derivation of the bubble energy relative to an elliptic deformation [40]:

$$\frac{l_c}{t} = S_{bs}(d) = \frac{1}{3} \left[ \frac{1}{2\pi} d^2 \left( \frac{16}{3} - L_{bs}(d) \right) - S_{bc}(d) \right] \quad (\text{A7})$$

with  $L_{bs}(d) = 16d \int_0^{\pi/2} (\sin^2 \alpha \cos^2 \alpha / \sqrt{1 + d^2 \sin^2 \alpha}) d\alpha$ .

The stripe-out diameter and field can be obtained in the same manner as the collapse diameter and field and are calculated to be and 1.96  $\mu\text{m}$  and 0.34 mT, respectively.

Finally, the saturation field for stripe domains is derived in [35] as follows:

$$1 - h_{s0} = \frac{1}{\pi} \left[ 2 \arctan(\omega_r) + \omega_r \ln \left( 1 + \frac{1}{\omega_r^2} \right) \right], \quad (\text{A8})$$

and it amounts to 0.38 mT.

- [1] C. D. Stanciu, F. Hansteen, A. V. Kimel, A. Kirilyuk, A. Tsukamoto, A. Itoh, and T. Rasing, All-Optical Magnetic Recording with Circularly Polarized Light, *Phys. Rev. Lett.* **99**, 047601 (2007).
- [2] A. Stupakiewicz, K. Szerenos, D. Afanasiev, A. Kirilyuk, and A. Kimel, Ultrafast nonthermal photo-magnetic recording in a transparent medium, *Nature (London)* **542**, 71 (2017).
- [3] A. V. Kimel and M. Li, Writing magnetic memory with ultra-short light pulses, *Nat. Rev. Mater.* **4**, 189 (2019).
- [4] M. L. M. Laliou, R. Lavrijsen, and B. Koopmans, Integrating all-optical switching with spintronics, *Nat. Commun.* **10**, 110 (2019).
- [5] N. Ogawaa, W. Koshibaea, A. J. Beekmana, N. Nagaosaa, M. Kubotaa, M. Kawasaka, and Y. Tokuraa, Photodrive of magnetic bubbles via magnetoelastic waves, *Proc. Natl. Acad. Sci. U.S.A.* **112**, 8977 (2015).
- [6] M. S. El Hadri, P. Pirro, C.-H. Lambert, S. Petit-Watelot, Y. Quessab, M. Hehn, F. Montaigne, G. Malinowski, and S. Mangin, Two types of all-optical magnetization switching mechanisms using femtosecond laser pulses, *Phys. Rev. B* **94**, 064412 (2016).
- [7] S. Alebrand, M. Gottwald, M. Hehn, D. Steil, M. Cinchetti, D. Lacour, E. E. Fullerton, M. Aeschlimann, and S. Mangin, Light-induced magnetization reversal of high-anisotropy TbCo alloy films, *Appl. Phys. Lett.* **101**, 162408 (2012).
- [8] G. Kichin, M. Hehn, J. Gorchon, G. Malinowski, J. Hohlfeld, and S. Mangin, From Multiple- to Single-Pulse All-Optical Helicity-Dependent Switching in Ferromagnetic Co/Pt Multilayers, *Phys. Rev. Appl.* **12**, 024019 (2019).
- [9] R. Medapalli, D. Afanasiev, D. K. Kim, Y. Quessab, S. Manna, S. A. Montoya, A. Kirilyuk, T. Rasing, A. V. Kimel, and E. E. Fullerton, Multiscale dynamics of helicity-dependent all-optical magnetization reversal in ferromagnetic Co/Pt multilayers, *Phys. Rev. B* **96**, 224421 (2017).
- [10] Y. Tsema, G. Kichin, O. Hellwig, V. Mehta, A. V. Kimel, A. Kirilyuk, and T. Rasing, Helicity and field dependent magnetization dynamics of ferromagnetic Co/Pt multilayers, *Appl. Phys. Lett.* **109**, 072405 (2016).
- [11] A. Kirilyuk, A. V. Kimel, and T. Rasing, Ultrafast optical manipulation of magnetic order, *Rev. Mod. Phys.* **82**, 2731 (2010).
- [12] S. Alebrand, A. Hassdenteufel, D. Steil, M. Bader, A. Fischer, M. Cinchetti, and M. Aeschlimann, All-optical magnetization switching using phase shaped ultrashort laser pulses, *Phys. Status Solidi A* **209**, 2589 (2012).
- [13] A. Ashkin and J. Dziedzic, Interaction of laser light with magnetic domains, *Appl. Phys. Lett.* **21**, 253 (1972).
- [14] A. Arora, M. A. Mawass, O. Sandig, C. Luo, A. A. Ünal, F. Radu, S. Valencia, and F. Kronast, Spatially resolved investigation of all optical magnetization switching in TbFe alloys, *Sci. Rep.* **7**, 9456 (2017).
- [15] K. Chesnel, A. S. Westover, C. Richards, B. Newbold, M. Healey, L. Hindman, B. Dodson, K. Cardon, D. Montealegre, J. Metzner, T. Schneider, B. Böhm, F. Samad, L. Fallarino, and O. Hellwig, Morphological stripe-bubble transition in remanent magnetic domain patterns of Co/Pt multilayer films and its dependence on Co thickness, *Phys. Rev. B* **98**, 224404 (2018).
- [16] L. Peng, Y. Zhang, D. Hong, B. Zhang, J. Li, J. Cai, S. Wang, J. Sun, and B. Shen, Spontaneous nanometric magnetic bubbles with various topologies in spin-reoriented La<sub>1-x</sub>Sr<sub>x</sub>MnO<sub>3</sub>, *Appl. Phys. Lett.* **113**, 142408 (2018).
- [17] N. Saratz, U. Ramsperger, A. Vindigni, and D. Pescia, Irreversibility, reversibility, and thermal equilibrium in domain patterns of Fe films with perpendicular magnetization, *Phys. Rev. B* **82**, 184416 (2010).
- [18] F. Büttner, M. A. Mawass, J. Bauer, E. Rosenberg, L. Caretta, C. O. Avci, J. Gräfe, S. Finizio, C. A. F. Vaz, N. Novakovic, M. Weigand, K. Litzius, J. Förster, N. Träger, F. Groß, D. Suzuki, M. Huang, J. Bartell, F. Kronast, J. Raabe *et al.*, Thermal nucleation and high-resolution imaging of submicrometer magnetic bubbles in thin thulium iron garnet films with perpendicular anisotropy, *Phys. Rev. Mater.* **4**, 011401(R) (2020).
- [19] L. Fallarino, A. Oelschlägel, J. A. Arregi, A. Bashkatov, F. Samad, B. Böhm, K. Chesnel, and O. Hellwig, Control of domain structure and magnetization reversal in thick Co/Pt multilayers, *Phys. Rev. B* **99**, 024431 (2019).
- [20] Tensormeter, “A new dimension of resistance measurements,” <http://tensormeter.eu/>, accessed December 2, 2019. [Online].
- [21] T. Kosub, M. Kopte, F. Radu, O. G. Schmidt, and D. Makarov, All-Electric Access to the Magnetic-Field-Invariant Magnetization of Antiferromagnets, *Phys. Rev. Lett.* **115**, 097201 (2015).
- [22] T. Kosub, S. Vélez, J. M. Gomez-Perez, L. E. Hueso, J. Fassbender, F. Casanova, and D. Makarov, Anomalous Hall-like transverse magnetoresistance in Au thin films on Y<sub>3</sub>Fe<sub>5</sub>O<sub>12</sub>, *Appl. Phys. Lett.* **113**, 222409 (2018).
- [23] F. Kronast and S. Valencia, SPEEM: The photoemission microscope at the dedicated microfocus PGM beamline UE49-PGMa at BESSY II, *J. Large-scale Res. Facil.* **2**, A90 (2016).
- [24] L. Gierster, L. Pape, A. A. Ünal, and F. Kronast, A sample holder with integrated laser optics for an ELMITEC photoemission electron microscope, *Rev. Sci. Instrum.* **86**, 023702 (2015).
- [25] C. M. Schneider and G. Schönhense, Investigating surface magnetism by means of photoexcitation electron emission microscopy, *Rep. Prog. Phys.* **65**, 1785 (2002).
- [26] S. Alebrand, A. Hassdenteufel, D. Steil, M. Cinchetti, and M. Aeschlimann, Interplay of heating and helicity in all-optical magnetization switching, *Phys. Rev. B* **85**, 092401 (2012).
- [27] P. Pershan, J. P. van der Ziel, and L. D. Malmstrom, Theoretical discussion of the inverse faraday effect, Raman scattering, and related phenomena, *Phys. Rev.* **143**, 574 (1966).
- [28] A. R. Khorsand, M. Savoini, A. Kirilyuk, A. V. Kimel, A. Tsukamoto, A. Itoh, and T. Rasing, Role of Magnetic Circular Dichroism in All-Optical Magnetic Recording, *Phys. Rev. Lett.* **108**, 127205 (2012).
- [29] Y. Quessab, Mechanism and size effects of helicity-dependent all-optical magnetization switching in ferromagnetic thin films, Ph.D. thesis, Université de Lorraine, 2018.
- [30] A. V. Kimel, A. Kirilyuk, P. A. Usachev, R. V. Pisarev, A. M. Balbashov, and T. Rasing, Ultrafast non-thermal control of magnetization by instantaneous photomagnetic pulses, *Nature (London)* **435**, 655 (2005).
- [31] K. Vahaplar, A. M. Kalashnikova, A. V. Kimel, S. Gerlach, D. Hinzke, U. Nowak, R. Chantrell, A. Tsukamoto, A. Itoh, A. Kirilyuk, and T. Rasing, All-optical magnetization reversal by circularly polarized laser pulses: Experiment and multiscale modeling, *Phys. Rev. B* **85**, 104402 (2012).
- [32] T. D. Cornelissen, R. Córdoba, and B. Koopmans, Microscopic model for all optical switching in ferromagnets, *Appl. Phys. Lett.* **108**, 142405 (2016).
- [33] S.-G. Je, P. Vallobra, T. Srivastava, J.-C. Rojas-Sánchez, T. H. Pham, M. Hehn, G. Malinowski, C. Baraduc, S. Auffret,

- G. Gaudin, S. Mangin, H. Béa, and O. Boulle, Creation of magnetic skyrmion bubble lattices by ultrafast laser in ultrathin film, *Nano Lett.* **18**, 7362 (2018).
- [34] O. Portmann, A. Vaterlaus, and D. Pescia, An inverse transition of magnetic domain patterns in ultrathin films, *Nature (London)* **422**, 701 (2003).
- [35] A. Hubert and R. Schäfer, in *Magnetic Domains, The Analysis of Magnetic Microstructures* (Springer-Verlag, Berlin, 1998), p. 700.
- [36] M. Kyselov, Phenomenological theories of magnetic multilayers and related systems, 1.7.2 Bubble Domains, Ph.D. thesis, Technical University Dresden, 2010.
- [37] S. I. Anisimov, B. L. Kapeliovich, and T. L. Perel'man, Electron emission from metal surfaces exposed to ultrashort laser pulses, *JETP* **39**, 375 (1974).
- [38] L. Belliard, J. Miltat, V. Kottler, V. Mathet, C. Chappert, and T. Valet, Stripe domains morphology versus layers thickness in CoPt multilayers, *J. Appl. Phys.* **81**, 5315 (1997).
- [39] N. Saratz, Inverse symmetry breaking in low-dimensional systems, Ph.D. thesis, ETH Zurich, 2009.
- [40] A. Thiele, Theory of the static stability of cylindrical domains in uniaxial platelets, *J. Appl. Phys.* **41**, 1139 (1970).